

## THE ASSEMBLY HISTORY OF GLOBULAR CLUSTER STAR STREAMS

RAYMOND G. CARLBERG

Department of Astronomy & Astrophysics, University of Toronto, Toronto, ON M5S 3H4, Canada  
*Draft version June 10, 2022*

### ABSTRACT

The early accretion onto the Milky Way of satellite galaxies containing dense star clusters is a likely source of the halo globular clusters and the beginning of their associated stellar streams. The process of infall of a satellite with dynamical friction and subsequent merging is simulated with a simple evolving potential model. King model clusters are initiated within the satellite galaxy on circular orbits in a disk. Merging places the clusters on new orbits that substantially underfill their tidal radii, requiring that some internal relaxation of the clusters must be included to cause them to expand to their new tidal surface and start or continue to produce star streams. A toy model with a simplified Monte Carlo relaxation procedure gives the clusters star particles random velocity kicks at approximately the rate expected from collisional dynamics. The clusters expand and lose stars to evaporation leading to tidal streams that have local properties, including sub-halo gaps, as expected in a static halo. The main difference is that the streams are, on the average, denser and lower velocity dispersion near to the clusters than they are further away, making the older parts of the streams relatively less visible. Comparing the numbers of dense stellar systems that likely formed and orbit within the range of galactic radii where streams are visible to the Pan-STARRS1 survey finds that the number of detected streams is comparable to the number of “lost” globular clusters above  $10^5 M_{\odot}$ , assuming that the detected streams follow the expectation that they arose from the most massive evaporated and evaporating clusters.

*Subject headings:* dark matter; Local Group; galaxies: dwarf; globular clusters; Galaxy: halo

### 1. INTRODUCTION

The study of tidal star streams emanating from globular clusters orbiting in the galactic potential is useful for measuring the shape of the galactic potential (Binney 2008; Law & Majewski 2010; Eyre & Binney 2011; Sanders & Binney 2013; Bovy et al. 2016b) and detecting the many dark sub-halos that are expected to be present (Klypin et al. 1999; Moore et al. 1999). The interaction of cluster tidal streams with sub-halos has been extensively studied in static potentials and is well understood in terms of the impact approximation (Ibata et al. 2002; Johnston et al. 2002; Yoon, Johnston & Hogg 2011; Carlberg 2012; Ngan et al. 2015; Sanders et al. 2016; Bovy et al. 2016a). In these studies a cluster is set on an orbit in a static galactic potential with the outer cluster radius usually adjusted to the local tidal radius at the apocenter of the orbit. The clusters are softened to be collisionless but in an reasonably elliptical orbit the tidal heating as the clusters go around pericenter is sufficient to cause mass loss. Although the mass loss rate varies around the orbit, it is periodic so that the the mean mass loss rate is constant and the dynamical properties of the stars along the stream repeat nearly exactly along the stream (Carlberg 2015a).

Much valuable insight results from the analysis of streams in a static potential but it also leads to some puzzles. For instance, globular clusters are 10 Gyr old systems with internal velocities of 1-10 km s<sup>-1</sup> that are close to the mean drift velocity down the stream, so should lead to long streams, 10-100 kpc, generally about half a wrap or more around the galaxy. However, streams like Pal 5 (Odenkirchen et al. 2001; Grillmair & Dionatos 2006b) still associated with a cluster, and, streams with no visible progenitor system, like GD-1 (Grillmair & Dionatos 2006a) have lengths of only 10 kpc or so. The length discrepancy for Pal 5 can be sidestepped if it only recently began losing stars but that runs counter to the idea that the halo globular clusters were incorporated into the galaxy before the disk of our galaxy began to substantially form. More generally it would be valuable to understand how the process of assembly of the globular clusters into our galactic halo affects the properties of the stellar streams, and, conversely, what insight stellar streams might provide into the history of the halo and its globular clusters.

Star formation that leads to current day dense star clusters that have masses and sizes of globular clusters occurs in galactic disks (Kravtsov & Gnedin 2005; Bournaud et al. 2008; Portegies Zwart et al. 2010; Renaud et al. 2016) and may be enhanced in vigorously star forming systems associated with mergers (Whitmore et al. 1999). The mass distribution of the dense stellar systems rises steeply,  $M^{-2}$ , and does not have the characteristic Gaussian shape of a globular cluster mass distribution. On the other hand there are strong arguments that the difference is a result of dynamical evolution.

The internal dynamical evolution of globular star clusters in a smooth galactic potential is fairly well understood (Spitzer 1987; Davies 2013) although it remains a lively subject. The mass evolution of globular clusters in the galaxy halo has been discussed at length (Fall & Rees 1977, 1985; Gnedin & Ostriker 1997; Fall & Zhang 2001; Gieles et al. 2011; Lamers et al. 2013). Here the emphasis is to how the history of globular cluster accretion into the Milky Way affects the stellar streams that they produce. All clusters are losing some stars though grav-

itational collision processes, but the rate of evaporation depends on the internal two body relation time and the local tidal field. The tidal field will evolve substantially for a cluster that is formed within the molecular clouds of the galactic disk and is later merged into the halo of a galaxy. And, as a cluster evaporates the properties of stars ejected into the tidal streams will also change, which in turn affects the density of the tidal stream created. Understanding the expected surface density of the tidal stream is an important practical consideration for detecting streams.

In this paper a toy model of accretion infall with dynamical friction of a satellite galaxy containing model clusters is developed. The satellite is represented as an evolving analytic potential in which the mass is dispersed over the host potential as it nears the center to approximate the merger of the two potentials into one. The particles in the model clusters are subjected to a simple Monte Carlo heating procedure which mimics the relaxation processes of globular clusters with the expected mass and size scaling. The evolution of the clusters with time and the resulting properties of the streams are presented. Finally, as motivated by these calculations, the number of star streams in the recent Pan-STARRS1 volume is compared to the number of globular clusters.

## 2. A SIMPLIFIED N-BODY MODEL

One of the reasons to use an analytic potential to study tidal streams emerging from globular star clusters is that there are no concerns that n-body particles are disturbing the streams which have internal velocities of only about  $1 \text{ km s}^{-1}$  around their mean motion of  $200 \text{ km s}^{-1}$ . Furthermore, there is no need in this exploratory study to have a full dynamical model of the merger process or detailed cosmological starting conditions. The requirement is for a satellite galaxy to fall into a host galaxy with a loss of energy and angular momentum sufficient to carry the globular cluster system fairly deep into the host galaxy potential after which the potential should become effectively stationary again.

The Milky Way 2014 model (Bovy 2015) is adopted as the initial host galaxy model, although the halo mass will be allowed to evolve. The potential does not respond to the infalling galaxy, which should be adequate here where the main purpose is to describe how the infall and accretion process alters the history of the tidal streams relative to a static model. A population of dark matter sub-halos is included, following the prescriptions of Carlberg & Grillmair (2016), although the sub-halos here extend fully out to 240 kpc with a cutoff at 360 kpc. Sub-halos below a mass of  $0.9 \times 10^7 M_{\odot}$  are not included because they make essentially no difference to the streams studied here.

### 2.1. The Satellite Starting Conditions

The infalling galaxy needs to have a well defined mass to allow the dynamical friction formula to be used. The Hernquist model,  $\phi_H(r, a) = -GM_H/(r + a)$  is a convenient choice (Hernquist 1990). For the Bovy MW2014 potential the halo mass inside the 245 kpc virial radius is 8.992 dimensionless units, where the mass unit is  $9.006 \times 10^{10} M_{\odot}$ . As a baseline satellite  $M_H$  is set to 2 units with  $a = 1.26$  which can be considered as a satellite with 22% of the mass of the host galaxy, although

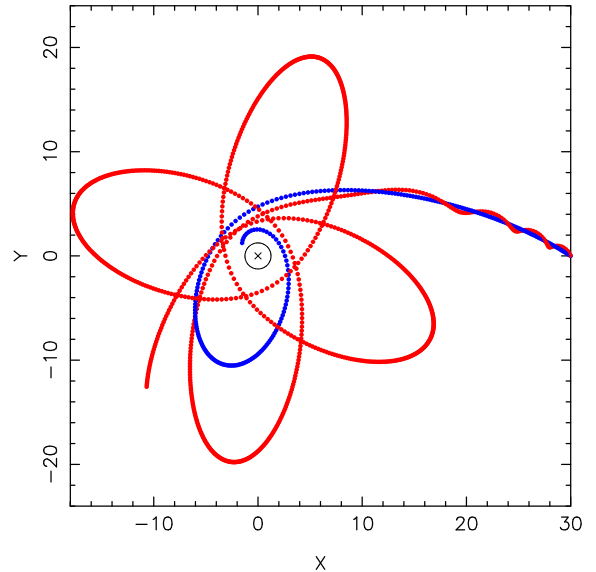


FIG. 1.— The blue points show the orbit of the center of the satellite potential with  $M_H = 0.3$ . The red points show the orbit of the center of a model star cluster. The scale is in the dimensionless units of 8 kpc per unit. More massive satellites sink more quickly with  $M_H = 2$  having only a quarter turn orbit.

the mass is not important here, only the resulting star cluster orbits.

Ideally the satellite galaxy orbit would be drawn from a cosmological simulation, but with a single infalling galaxy all that is required is a reasonably representative starting point someplace near the virial radius. The satellite galaxy is started in a bound orbit, at a galactocentric  $x$  of 240 kpc and above the plane of the MW2014 model at  $z$  of 120 kpc. The satellite is given an initial tangential velocity equal to 0.35 of the local circular velocity and an inward radial velocity of 0.61 of the local circular velocity.

### 2.2. The Merger Model

A simple evolving potential model is needed to deliver the star clusters into the inner galaxy on orbits with a range of eccentricities. An accurate violent relaxation model is not essential for this investigation which focuses on the star clusters. The satellite potential falls into the host galaxy with the motion of its center calculated from the host potential with the addition of dynamical friction. Chandrasekhar's formula (Binney & Tremaine 2008; Boylan-Kolchin et al. 2008) is used to evaluate the dynamical friction, with  $\ln \Lambda = 10$  adopted. Only the NFW dark matter halo of MW2014 is used to calculate the local density for friction. For the friction calculation the MW2014 halo is given a small core radius equal to the MW2014 bulge core radius to avoid a singularity when the satellite potential is dragged to the center of the host galaxy.

Dynamical friction draws the satellite into the center in about a dynamical time. In an n-body system, the outer parts of the satellite become unbound, spreading out into the host galaxy potential. To approximate this process, the satellite potential needs to lose mass and expand to spread over the host halo potential. The key

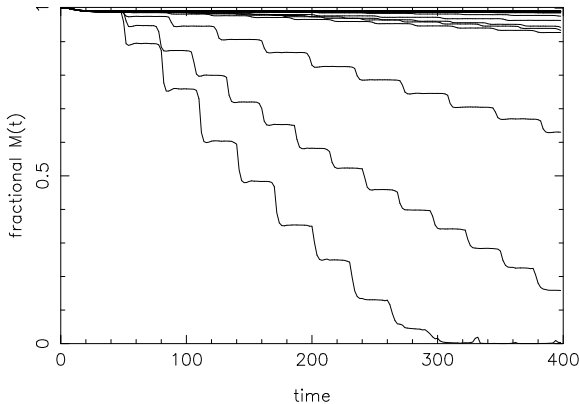


FIG. 2.— Mass as function of time for the 24 clusters each with mass  $0.9 \times 10^5 M_\odot$  with no additional relaxation process.

quantity is  $\Omega_s$ , the local circular frequency of the satellite orbit, which is calculated from the local acceleration in the host galaxy,  $\Omega_s = \sqrt{\mathbf{a} \cdot \mathbf{r}/r}$ . The spread in circular frequency of the orbit at radius  $r$  across the scale radius of the satellite,  $a$ , is  $\delta\Omega_s \simeq \Omega_s a/r$ . Therefore, the rate of satellite mass decrease due to orbital divergence is  $dM_s/dt \simeq M\delta\Omega_s$ . The scale radius of the satellite,  $a$ , expands as  $da/dt \simeq r\delta\Omega_s$ . In the implementation of these ideas, the maximum scale radius of the satellite is limited to 5 times the scale radius of the NFW of the host galaxy. The mass taken from the satellite is added to the host galaxy halo without changing its scale radius. Under this process the satellite orbits into the center of the host galaxy, expanding in size and with its mass going to zero. The mass lost is added to the host galaxy NFW potential. An example merger orbit is shown in Figure 1 for an  $M_H = 2$  satellite, roughly 22% of the host galaxy mass, although any precise satellite mass identification is uncertain.

### 2.3. Initial Star Cluster Distribution

The star clusters are King models, all with a fairly conventional King model concentration parameter of  $W_0 = 4$ . A set of 24 star clusters is placed on circular orbit within the infalling galaxy, 12 at  $r_H$  and 12 at  $r_H/2$ . The outer radii of the clusters are set equal to the local tidal radius, calculated using a tidal mass  $GM_t = r \mathbf{a} \cdot \mathbf{r}$  where the acceleration is calculated from the satellite potential alone. The clusters are in a disk that can be tilted, usually at  $45^\circ$ , with respect to the plane of the host galaxy potential. The cluster particles are evolved with a shell gravity code which accurately reproduces the results of a full n-body code (Carlberg 2015b).

In physical terms, the clusters begin within about 10 kpc of the center of their satellite host, which is itself at a distance of about 250 kpc from the center of the main host galaxy. Figure 1 shows a typical infall event for a single cluster. The cluster orbits around the center of the infalling galaxy which is losing mass and expanding as it falls in. The mass drops to half at a galactocentric

radius of 5-10 units with the satellite becoming effectively at that time. Once the cluster orbit separates from the infalling galaxy the cluster underfills its tidal radius until heating can expand it. The satellite galaxy in Figure 1 has  $M_H = 0.3$ . A satellite with  $M_H = 2$  makes only a one quarter turn orbit before plunging to the center.

### 2.4. A Simple Model of Cluster Internal Dynamics

During the satellite's infall into the host the clusters cease to orbit the satellite and begin to orbit in the host at 30-50 kpc, as is shown for a single cluster in Figure 1. The tidal field is usually much weaker on the new orbit than it was on the orbit within the satellite. Consequently, most of the clusters will not extend to their tidal radii in the merged system. The King model clusters contain particles with a sufficiently large softening and large enough particle counts that they are effectively collisionless. Hence, with only weak tidal heating, evaporation of star particles will largely cease as shown in Figure 2, independent of mass. The clusters need to be given the internal relaxation processes that gravitational interactions cause to provide more realistic behavior.

The internal dynamics of globular clusters are a rich subject which continues to develop both with ever more realistic n-body simulations and dynamical analysis. The evolution of star clusters is reviewed in (Spitzer 1987; Binney & Tremaine 2008; Davies 2013). In brief, two body relaxation leads to the core shrinking and envelope expansion until heating from central binary and multiple star systems usually intervenes to at least partially reverse core collapse and sometimes cause core oscillations. The gravitational collisions, largely in the central region, cause stars in the envelope to gradually move to larger orbits until they reach a tidal surface and flow away from the cluster. Gieles et al. (2011) find that clusters with mass greater than  $(8 \text{ kpc}/r)4 \times 10^4 M_\odot$ , are in the expansion dominated phase of evolution, where  $r$  is the galactocentric radius of the cluster. Streams have generally been found outside the solar circle at a minimum and usually twice that radius. By the above criterion a typical halo cluster at 15 kpc that is more massive than  $2 \times 10^4 M_\odot$  will be in the expansion phase of evolution for their lifetime.

The controlling timescale for internal evolution of a cluster of mass half mass  $M_{1/2}$  is the relaxation time at the half mass radius,  $r_{1/2}$ ,

$$t_{rh} \propto M_{1/2}^{1/2} r_{1/2}^{3/2} \propto \sqrt{\langle v^2 \rangle} r_{1/2}^2 \quad (1)$$

(Spitzer 1969, 1987), where  $\sqrt{\langle v^2 \rangle}$  is a representative half-mass velocity dispersion. The relaxation process causes the outer 70-90% of the cluster mass to expand (Freitag et al. 2006a,b) with the inner regions remaining at roughly constant size.

This paper is primarily oriented towards understanding the entire history of the creation of tidal tails. The approach is to provide small velocity increments to stars beyond some critical mass radius so that,

$$\frac{d\langle v^2 \rangle}{dt} = \frac{\langle v^2 \rangle}{t_{rh}(M_{1/2}, r_{1/2})}. \quad (2)$$

In this approach energy is being added to the system, which in a dynamically correct simulation would be ex-

tracted from the shrinking core and later from binary and multiple systems (Giersz 1998). The focus here is on envelope expansion, which requires a source of internal energy, which for this initial investigation the details of its source is set aside. The velocity increments,  $\delta v$ , are applied at discrete intervals,  $\delta t_r$ . Over the duration of the simulation,  $T$ , the velocity gains are  $\Delta\langle v^2 \rangle = T/\delta t(\delta v)^2$ . Comparing Equations 1 and 2 gives the required step-wise velocity changes,

$$(\delta v)^2 \propto \frac{\delta t}{T} \frac{M_{1/2}^{1/2}}{r_{1/2}^{5/2}}. \quad (3)$$

A practical implementation of Equation 3 is every  $\delta t$  in time to add random velocities drawn from a Gaussian distribution of width,

$$\delta v = C\sigma \left(\frac{\delta t}{T}\right)^{1/2} \left(\frac{M_{1/2}}{10^{-7}}\right)^{1/4} \left(\frac{r_{1/2}}{10^{-3}}\right)^{-5/4}, \quad (4)$$

in the dimensionless units of the calculation, where  $C$  is a constant around unity and  $\sigma$  is a representative velocity dispersion, about  $1 \text{ km s}^{-1}$  for scaling, or  $1/220$  in the dimensionless units of the calculation. The  $\delta v$  value is used to generate random velocity offsets in the  $xyz$  directions from a Gaussian distribution.

A little experimentation is required to fine tune the various quantities that need to be calculated and the parameters controlling the process. An outer radius for the evaluation of the RMS velocity and the half mass radii of the clusters is selected to  $r_m = 0.02$  units (160 pc) which is somewhat larger than the initial tidal radius of the clusters. No heating is done for particles beyond  $r_m$  or inside the radius containing  $1/3$  of the mass inside  $r_m$ , the latter to roughly replicate the results of detailed collisional n-body models. The heating calculation is done every  $\delta t$  of 100 steps ( $0.71 \times 10^7$  yr) Equation 4 is evaluated with  $C\sigma\sqrt{\delta t/T}$  set equal to  $3 \times 10^{-4}$ . The simulations usually lasts 200,000 steps so this random walk process happens 2000 times, although a larger number of smaller steps would lead to the same outcome.

### 3. CLUSTER DISSOLUTION IN A MERGING SYSTEM

The main set simulations presented here has 24 star clusters at each of three cluster masses at  $0.9 \times 10^4 M_\odot$ ,  $0.9 \times 10^5 M_\odot$  and  $0.9 \times 10^6 M_\odot$ . All satellite galaxies start from the same location near the virial radius, with a modest amount of angular momentum. The main simulations put the clusters in a satellite galaxy with  $M_H = 2$  which can be considered a 22% mass satellite. The simulations run for 400 time units, or 14.2 Gyr, which is a little beyond the Hubble age, but the outcomes are substantially the same at earlier times. All simulations use the same heating parameters and merger model. Simulations have been run for many other satellite masses, satellite starting conditions, sub-halo contents of the host galaxy and the cluster internal relaxation parameters, however the set presented provides a good guide to many other situations.

Figure 3 shows the fractional cluster mass as a function of time for three initial masses of  $0.9 \times 10^4 M_\odot$ ,  $0.9 \times 10^5 M_\odot$  and  $0.9 \times 10^6 M_\odot$ , from top to bottom, respec-

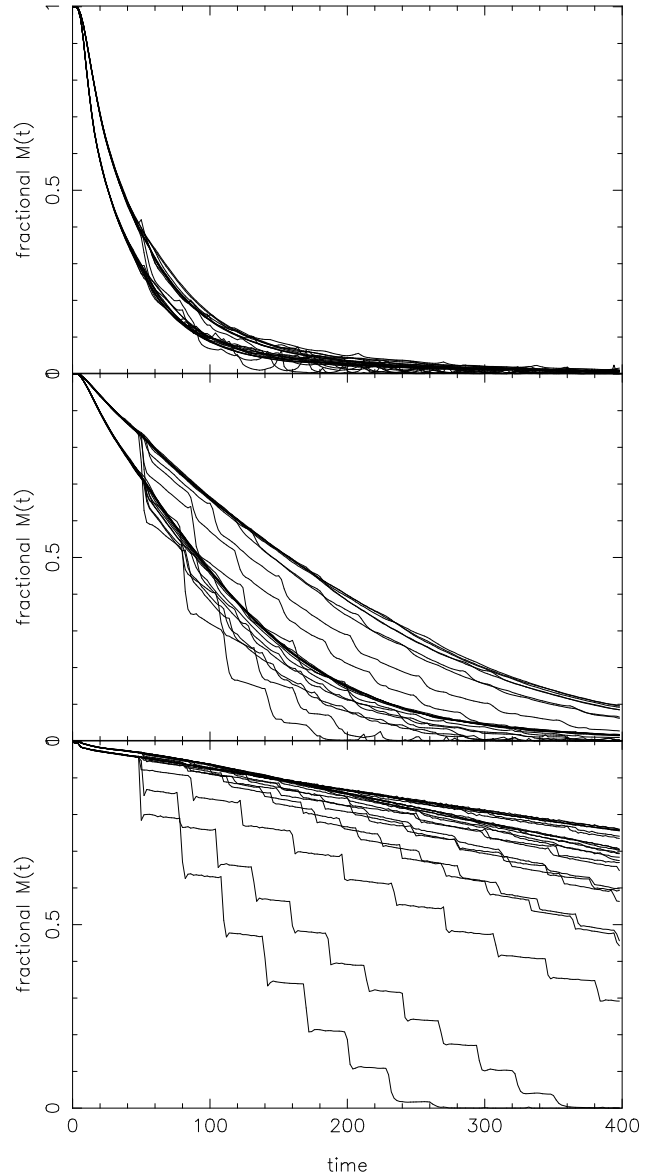


FIG. 3.— Mass as function of time for the 24 clusters each with mass  $0.9 \times 10^4, 10^5, 10^6 M_\odot$  in the top, middle and bottom panels, respectively. The relaxation model is incorporated into all of these, with the same parameters for all. Highly eccentric orbits have large mass loss variations around the orbit.

tively. The envelope heating model of Equation 4 is active in all these clusters. The middle panel is for the same clusters as in Figure 2, which had no internal relaxation. The  $0.9 \times 10^4 M_\odot$  clusters in the top panel have relaxation driving the evaporation of the cluster, with only a minimal dependence on the cluster orbits which drives tidal heating. The clusters in the top panel clearly separate into the 12 inner and 12 outer clusters, with the inner group being somewhat denser and hence having a shorter relaxation time, Equation 2. The lower panel is for the most massive clusters simulated,  $0.9 \times 10^6 M_\odot$ , where relaxation is of reduced importance, with tides now playing a much more important role. Two of the 24 clusters of the bottom panel have sufficiently elliptical orbits that tidal fields help drive complete evaporation.

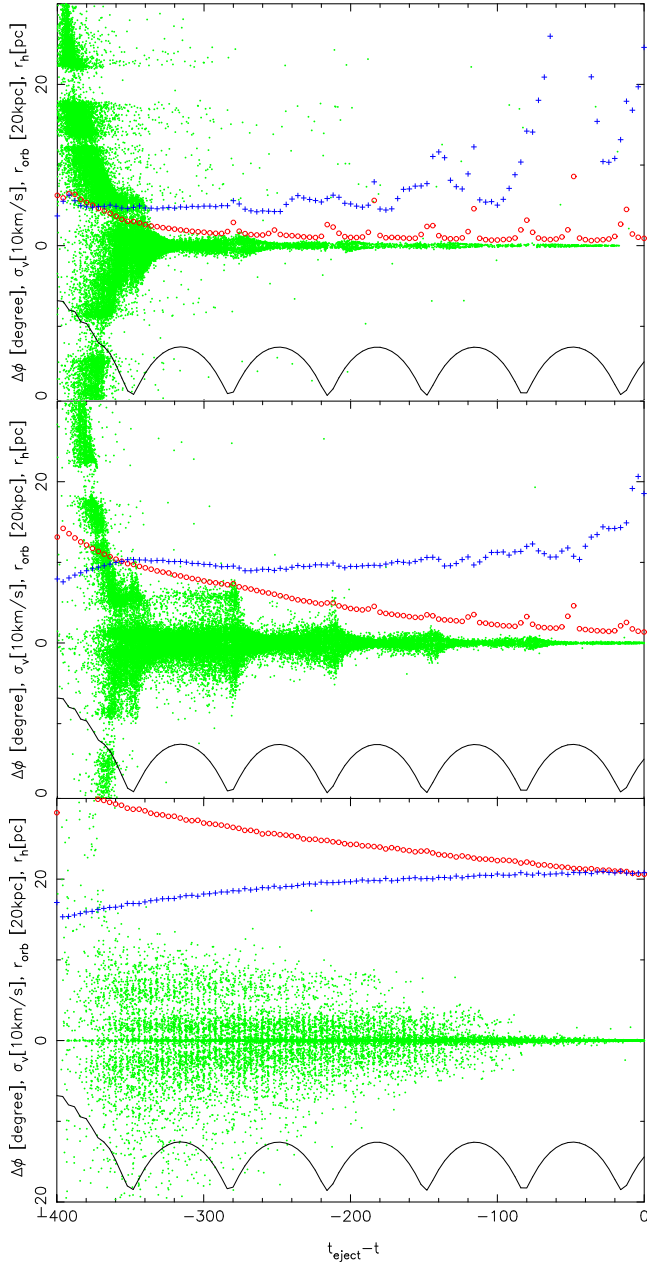


FIG. 4.— Evolution of the satellite and particles released into the stream with time for single clusters on the same orbit with mass  $0.9 \times 10^4$ ,  $10^5$ ,  $10^6 M_\odot$  in the top, middle and bottom panels, respectively. Red circles are the 3D velocity dispersion in  $\text{km s}^{-1}$  times 10. Blue plus signs are the half mass radius of the remaining star cluster in parsecs. Green is the angular distance on the sky between the satellite center and the released particles, measured in degrees. Red line is the dimensionless orbital radius in 20 kpc units, offset by -20 to the bottom of the plot.

The characteristic dynamical quantities of a single cluster and its stream are illustrated in Figure 4 as a function of time for individual clusters at masses  $0.9 \times 10^4$ ,  $0.9 \times 10^5$  and  $0.9 \times 10^6 M_\odot$  clusters, from top to bottom, respectively. The clusters are all on exactly the same orbit. All three clusters exhibit the similar basic behavior but with differences of scale. The cluster half mass radius expands about 50% over the lifetime of the cluster and the

velocity dispersion drops essentially to zero if the cluster evaporates completely. Since the half mass radius does not vary a lot with time until the cluster is nearly completely evaporated, the variation with time of a cluster is largely driven by its mass, or equivalently, velocity dispersion. The spray of (green) points shows the current distance from the progenitor cluster (or its remnant center) as a function of the time at which the star particle went through the tidal surface. The lowest mass cluster loses relatively more stars when the cluster was still in the satellite galaxy. These stars spread to relatively large angular distances away from the progenitor cluster. The particles that evaporate late do so at such low velocity dispersions that they remain close to the cluster. The most massive set of clusters lose relatively few stars while in the satellite, after which the clusters maintain a fairly uniform low rate of mass loss ejecting stars at velocities that only allows particles to reach distances of  $20^\circ$  or so from the cluster.

The mean particle density distribution in the streams is plotted as function of azimuthal angle with the orbit projected onto the x-y plane in Figure 5 for the 24 clusters at  $0.9 \times 10^4$ ,  $0.9 \times 10^5$  and  $0.9 \times 10^6 M_\odot$  clusters, from top to bottom, respectively. As a log of density versus angle plot, a linear decline corresponds to an exponential decline of density with angle. Because all cluster models have 50,000 star particles, the actual stellar density needs to take the conversion from particle mass to star mass into account. Both the  $0.9 \times 10^4 M_\odot$  and the  $0.9 \times 10^5 M_\odot$  clusters nearly completely evaporate to produce similar streams. Hence, the more stars in the cluster, the more stars in the stream although this is moderated by the increased velocity dispersion and length, which both scale as the tidal radius, or,  $M_c^{1/3}$ . Consequently a ten times more massive cluster will lead to about a 2.1 times higher surface density which will be easier to find on the sky.

The density profiles (in particle counts) of individual streams from the inner dozen clusters at  $0.9 \times 10^4$ ,  $0.9 \times 10^5$  and  $0.9 \times 10^6 M_\odot$  clusters is shown in Figure 6, from top to bottom, respectively. First, the considerable variation of the stream density profiles from one orbit to the next is clearly visible. Second, the sub-halo induced gaps are readily visible in the upper two panels. Because the orbits of both clusters and sub-halos are the same for the two sets of cluster masses the gaps are very similar, although there are differences of details because the streams have different dynamical structures. The readily visible gaps range in size from a degree up to about ten degrees, with the most visible gaps being around 5 degrees in length.

On the basis of these simulations a Pal 5 progenitor would need to be somewhat heavier than  $10^5 M_\odot$  to avoid complete cluster evaporation although the stream could become a reasonable model for GD-1 which has no known progenitor. In either case about half of the individual streams in Figure 6 in the top and middle frames show density profiles that are fairly flat and contain a few large gaps, approximately as is claimed to be visible in some known streams on the sky.

#### 4. VISIBILITY OF STREAMS ON THE SKY

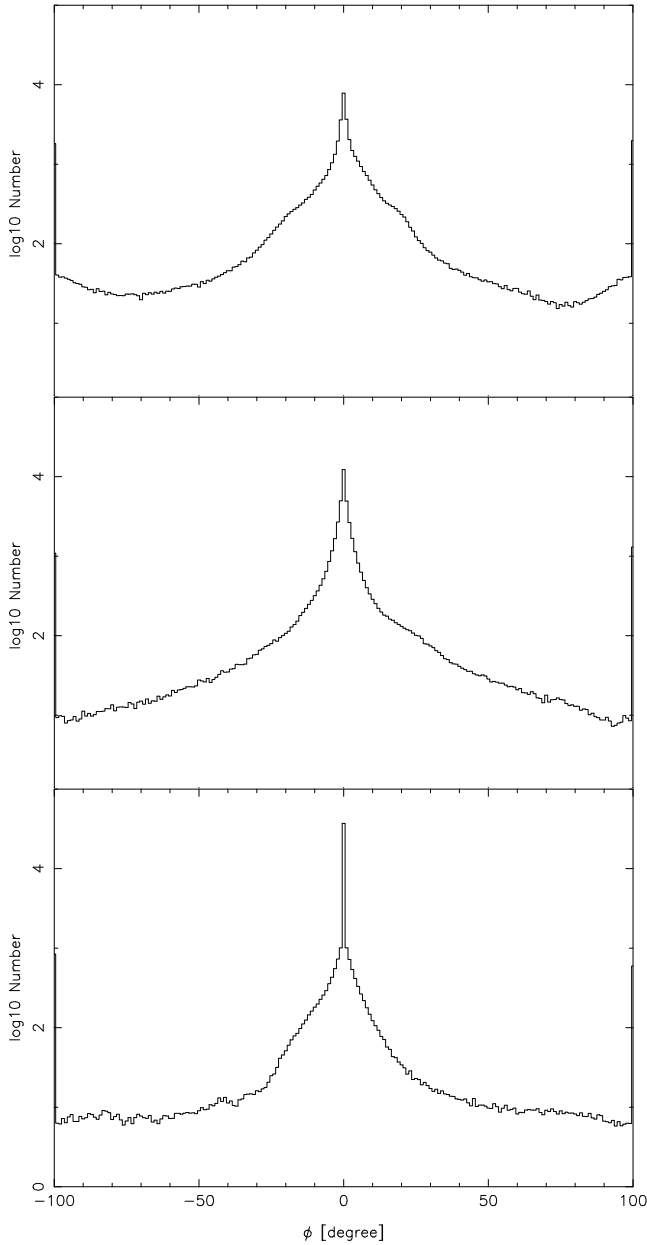


FIG. 5.— The average particle density along the stream projected onto the x-y plane averaging together 24 clusters with mass  $0.9 \times 10^4, 10^5, 10^6 M_\odot$  in the top, middle and bottom panels, respectively.

The simulations here lead to star clusters at masses around  $10^6 M_\odot$  evaporate slowly and produce streams with relatively high velocity dispersion making them proportionally somewhat wider and less visible on the sky. Clusters at masses around  $10^4 M_\odot$  evaporate completely, but, they have fewer stars. Clusters around  $10^5 M_\odot$  are the most massive clusters to evaporate almost completely so they have a fair number of stars and produce relatively dense star streams. Therefore the most readily detectable streams should come from this group of clusters that are the most massive to evaporate almost completely.

The effects of sub-halos on streams is illustrated in

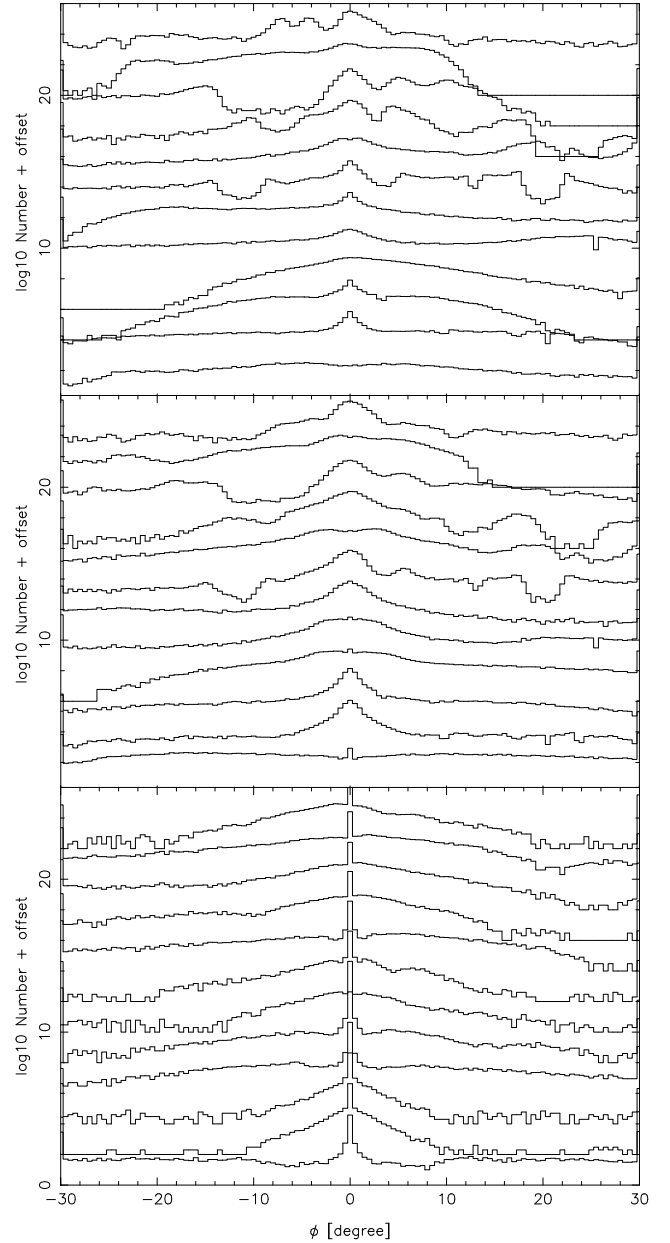


FIG. 6.— The density along the stream for individual streams from the 12 inner clusters with masses  $0.9 \times 10^4, 10^5, 10^6 M_\odot$  in the top, middle and bottom panels, respectively. The density variations are the result of sub-halos passing through the streams.

Figure 7 where 24 clusters of mass  $0.9 \times 10^5 M_\odot$  without (top panel) and with sub-halos present (bottom panel) are shown. In this plot any pixel with a particle becomes black. This particular simulation uses a very high satellite,  $M_H = 8$  to put most of the clusters in the inner region of the galaxy. The infall orbit also produces a fair number of clusters on relatively high eccentricity orbits. Although the sub-halos certainly act to create density variations in the streams, the streams themselves remain substantially intact. That is, they are not blurred out into a smooth halo distribution.

Streams are very low sky density features which in photometric data alone usually only become detectable

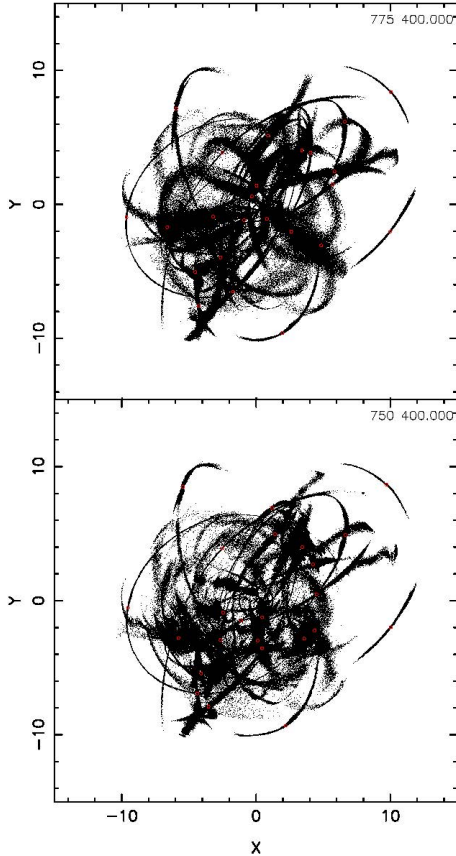


FIG. 7.— The tidal tails of a set of 24 infalling clusters each with mass  $0.9 \times 10^5 M_{\odot}$  without (top panel) and with (bottom panel) sub-halos present. The satellite has  $M_H = 8$  which brings almost all the clusters into the inner halo. The grid scale is in units of 8kpc. The red circles are the locations of the nominal cluster centers, some of which have no remnant cluster.

through the use of color-magnitude diagram filtering (Rockosi et al. 2002) which optimally weights some desired common age, metallicity and distance population of stars in preference to field stars. Even with such procedures currently available data generally lead to streams with a signal-to-noise per degree length of stream of a few. If the stream is at a sufficiently large distance such that the large number of stars near the turnoff from the main sequence are not within the sample, about 20 kpc for current images, then the signal to noise drops further. The outcome is that finding star streams is difficult at best and essentially impossible with current data to detect lower density regions of streams.

In Figure 8 the sky density is shown for all 24 streams of the bottom panel of Figure 7 with sub-halos. In the upper panel of Figure 8 any pixel on the sky with a star is black, irrespective of the numbers. A pixel is 0.002 units in a the Aitoff-Hammer coordinate which has a maximum of  $2\sqrt{2}$ . Scaling to  $360^\circ$  indicates that the pixels are approximately  $0.13^\circ$  on a side. To more accurately represent sky density, in the bottom panel the pixel density is de-weighted with the inverse distance squared for stars beyond 16 kpc and the resulting pixel density plotted with a grey scale from 0 to 10 units.

The weighted map of the sky density of streams is a much more realistic view of what should be expected

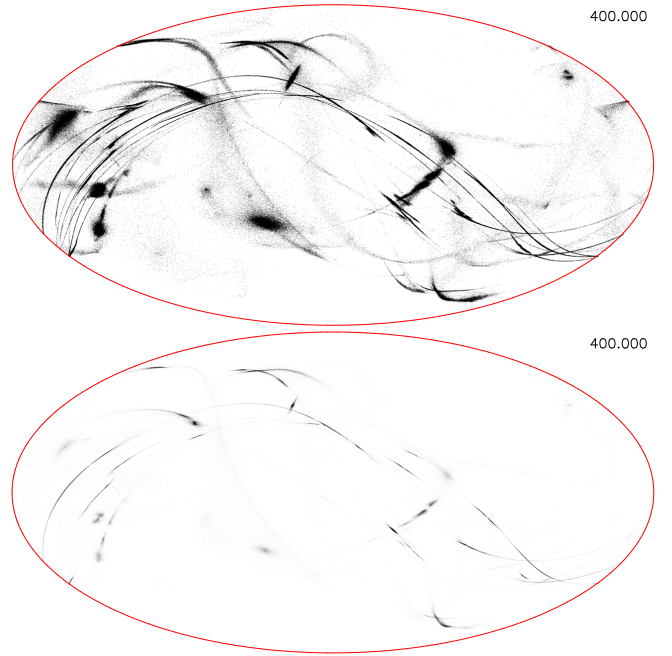


FIG. 8.— The Aitoff-Hammer projection of the 24 clusters of  $0.9 \times 10^5 M_{\odot}$  in the  $M_H = 8$  infall model with all particles equally visible (top panel) and sky densities stretched over a grey scale range of 0-10 and particles beyond 16 kpc weighted by their inverse distance squared (bottom panel).

in current sky maps (Ngan et al. 2015). The streams are thinner and shorter than they would be if all stars were detected, which will eventually be possible. The key factor is that streams do not disappear entirely. That is, even though the length and width of streams is likely being under-estimated, the counts of streams is likely to be accurate for streams within the turn-off detection distance. The details of the stream selection function will be studied more quantitatively in a future paper.

## 5. COUNTS OF STREAMS AND CLUSTERS

The mass distribution of dense star clusters, which are plausible low-redshift analogs of the progenitors of globular clusters, is approximately  $M^{-2} \exp(-M/M_*)$  (Portegies Zwart et al. 2010). The most massive clusters to evaporate, those around  $10^5 M_{\odot}$  will produce the most luminous streams which will be the easiest to detect, all else being equal. Together these ideas suggest a consistency test of the idea of that the progenitor cluster distribution varies as  $M^{-2}$  is that the sum of the numbers of globular clusters and the numbers of streams to some mass limit should add up to the progenitor numbers. That is, the streams are the “lost” clusters, predominantly the most massive ones, although the test is weakened by the lack of accurate and likely incomplete stream stellar masses.

The PS1- $3\pi$  survey allows a fairly uniform comparison of star streams to the known globular clusters, as represented in the Harris (1996) catalog. Within the PS1- $3\pi$  sky Bernard et al. (2016) recover 9 previously known thin streams (wider, dwarf galaxy streams are excluded here), and, find 5 new ones for a total of 14. A few additional streams are known in this sky area, but the PS1- $3\pi$  provides a uniform basis for selection. The remnant halo

clusters are those visible within the same sky volume as star streams are found. The sky volume is north of Declination  $-30$ , a galactocentric radius of less than 35 kpc, which is the maximum distance that PS1- $3\pi$  searches for streams, and at a galactocentric radius greater than 10 Kpc, inside of which streams are rare, likely because they encounter the baryonic structures of the disk and are eroded. To a first approximation the obscuration of the galactic disk should be about the same for streams and the halo population of globular clusters. To select halo globular clusters, an upper limit on metallicity of  $[\text{Fe}/\text{H}]$  of  $-1$  is imposed, although this only eliminates 3 very low luminosity clusters out of 27. Masses are assigned to the globular clusters using a uniform M/L of 2 solar units and are plotted in Figure 9. The set of clusters selected have a mean galactocentric distance of 19 kpc.

The mass distribution of current epoch dense star clusters is a steep power law, approximately  $M^{-2}$ . In Figure 9 the dashed line is  $7(M/M_*)^{-1} \exp(-M/M_*) \Delta M/M$  with  $M_* = 10^6 M_\odot$  and  $\Delta \log_{10} M = 0.2$ , which approximately fits the mass distribution of the half dozen clusters above  $3 \times 10^5 M_\odot$ . The dotted histogram is the cumulative difference between the clusters observed to be present and their assumed progenitor numbers, that is, the number of “lost” clusters. The difference between the 28.6 clusters expected from the dense star cluster progenitor distribution and the 14 clusters more massive than  $10^5 M_\odot$  is 14.6. The number of PS1 streams is 14. Given the small numbers, particularly for the normalization of the expected numbers, which is based on half a dozen clusters, the degree of agreement should not be over-interpreted. Although only a few streams have a measured mass, it is likely to be a lower limit. In any case, it is reasonable to assume that Bernard et al. (2016) are seeing the most massive evaporated clusters, since those will have the most stars. If the selection function drops off steeply for streams below  $10^5 M_\odot$  then the 14 thin streams in the PS1- $3\pi$  volume are the “lost” clusters above  $10^5 M_\odot$ , which is the basis for placing the pincushion symbol in Figure 9. Of course if the streams have their origin in somewhat lower mass progenitor clusters then most of the “lost” clusters are not currently found as star streams. Certainly there should be many more fainter streams to be found, even in the relatively accessible volume of the PS1- $3\pi$ , even if the progenitor cluster mass distribution is not as steep as  $M^{-2}$ .

## 6. DISCUSSION

This paper takes a step towards a more accurate description of the creation of a star stream as a result of the tidal evaporation of a star cluster that is formed in a satellite galaxy that subsequently merges into a Milky Way potential. Once the star cluster is freed from the satellite it usually finds itself on an orbit of significantly lower tidal fields. If the particles in the cluster are effectively collisionless, little mass loss occurs. Accordingly this paper develops a toy model with a simple merger and heating functions with the expected scaling for the internal dynamics of star clusters. The outcome is that clusters expand and cool as they lose mass, causing the stream density to vary with distance. The result is an

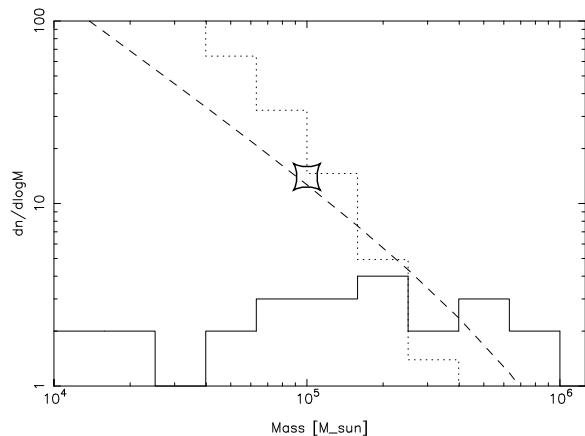


FIG. 9.— The number of globular clusters as a function of mass in the PS1- $3\pi$  survey (solid histogram) compared to the number of dense stellar systems expected to be formed in an  $M^{-2} \exp(-M/M_*)$  distribution normalized to the top half dozen clusters (dashed line). The dotted histogram is the cumulative sum of the difference between the assumed initial distribution and the current numbers, which are expected to become stellar streams. The pincushion symbol is for the 14 streams recovered in the PS1- $3\pi$  area. The few stream masses known are in the few  $\times 10^4 M_\odot$  range. The streams are put at  $10^5 M_\odot$  primarily on the basis that the heaviest “lost” clusters should be the most visible star streams so the stream mass should be as high as allowed.

improved understanding of stream structure for a more realistic assembly history, although almost every aspect of the simulation can be improved in more detailed future investigations.

Model clusters having a mass around  $10^6 M_\odot$  lose about one third of their mass in a Hubble time and  $10^5 M_\odot$  clusters largely evaporate in about 2/3 of a Hubble time. The resulting stellar streams have an approximately exponential density profile with azimuth within  $30-40^\circ$  on the sky of the progenitor, although there is considerable case to case variation. The oldest part of the stream is nearly constant density. When projected onto the sky, the decline of the mean density away from the progenitor helps explain why the readily visible parts of most streams are relatively short, even though the simulated streams often wrap a good fraction of their orbit around the galaxy. Although dark matter sub-halos create gaps along the streams those are largely azimuthal changes so the streams as a whole remains robust structures (Helmi & White 1999).

The PS1- $3\pi$  survey finds 14 streams (Bernard et al. 2016). In the same sky volume there are 14 globular clusters to  $10^5 M_\odot$ , whereas an  $M^{-2}$  distribution would predict about 28. If the known stream are the most massive streams, they then can fully account for the 14 “lost” clusters that an  $M^{-2}$  cluster mass distribution would contain down to about  $10^5 M_\odot$ . The key assumption here is that all these streams really do have total masses above  $10^5 M_\odot$  which is certainly not verified. In any case, if a steep progenitor mass distribution is true then many more lower mass streams should be discovered as the halo is better mapped, since the streams remain



as coherent structures.

Future work on the assembly of globular clusters into the galaxy and the development of streams will improve many aspects of these simulations. Cosmological starting conditions will be used, along with a full n-body model to follow the gravity field and the internal dynamics of the clusters can incorporate a more complete description.

A goal is to place the simulation outcomes into the sky and compare to the observed globular clusters and star streams.

This research was supported by CIFAR and NSERC Canada.

## REFERENCES

- Bernard, E. J., Ferguson, A. M. N., Schlafly, E. F., et al. 2016, MNRAS,
- Binney, J. 2008, MNRAS, 386, L47
- Binney, J., & Tremaine, S. 2008, *Galactic Dynamics: Second Edition*, Princeton University Press
- Bournaud, F., Duc, P.-A., & Emsellem, E. 2008, MNRAS, 389, L8
- Bovy, J. 2015, ApJS, 216, 29
- Bovy, J., Erkal, D., & Sanders, J. L. 2016, arXiv:1606.03470
- Bovy, J., Bahmanyar, A., Fritz, T. K., & Kallivayalil, N. 2016, arXiv:1609.01298
- Boylan-Kolchin, M., Ma, C.-P., & Quataert, E. 2008, MNRAS, 383, 93
- Carlberg, R. G. 2012, ApJ, 748, 20
- Carlberg, R. G. 2015a, ApJ, 800, 133
- Carlberg, R. G. 2015b, ApJ, 808, 15
- Carlberg, R., & Grillmair, C. 2016, arXiv:1606.05769
- Davies, M. B. 2013, *Planets, Stars and Stellar Systems. Volume 5: Galactic Structure and Stellar Populations*, 5, 879
- Eyre, A., & Binney, J. 2011, MNRAS, 413, 1852
- Fall, S. M., & Rees, M. J. 1977, MNRAS, 181, 37P
- Fall, S. M., & Rees, M. J. 1985, ApJ, 298, 18
- Fall, S. M., & Zhang, Q. 2001, ApJ, 561, 751
- Freitag, M., Gürkan, M. A., & Rasio, F. A. 2006, MNRAS, 368, 141
- Freitag, M., Rasio, F. A., & Baumgardt, H. 2006, MNRAS, 368, 121
- Gieles, M., Heggie, D. C., & Zhao, H. 2011, MNRAS, 413, 2509
- Giersz, M. 1998, MNRAS, 298, 1239
- Gnedin, O. Y., & Ostriker, J. P. 1997, ApJ, 474, 223
- Grillmair, C. J., & Dionatos, O. 2006a, ApJ, 643, L17
- Grillmair, C. J., & Dionatos, O. 2006b, ApJ, 641, L37
- Harris, W. E. 1996, AJ, 112, 1487
- Helmi, A., & White, S. D. M. 1999, MNRAS, 307, 495
- Hernquist, L. 1990, ApJ, 356, 359
- Ibata, R. A., Lewis, G. F., Irwin, M. J., & Quinn, T. 2002, MNRAS, 332, 915
- Johnston, K. V., Spergel, D. N., & Haydn, C. 2002, ApJ, 570, 656
- Klypin, A., Kravtsov, A. V., Valenzuela, O., & Prada, F. 1999, ApJ, 522, 82
- Kravtsov, A. V., & Gnedin, O. Y. 2005, ApJ, 623, 650
- Lamers, H. J. G. L. M., Baumgardt, H., & Gieles, M. 2013, MNRAS, 433, 1378
- Law, D. R., & Majewski, S. R. 2010, ApJ, 714, 229
- Moore B., Ghigna S., Governato F., et al., 1999a, ApJL, 524, L19
- Navarro, J. F., Frenk, C. S., & White, S. D. M. 1997, ApJ, 490, 493
- Ngan, W., Bozek, B., Carlberg, R. G., et al. 2015, ApJ, 803, 75
- Odenkirchen, M., Grebel, E. K., Rockosi, C. M., et al. 2001, ApJ, 548, L165
- Portegies Zwart, S. F., McMillan, S. L. W., & Gieles, M. 2010, ARA&A, 48, 431
- Renaud, F., Agertz, O., & Gieles, M. 2016, arXiv:1610.03101
- Rockosi, C. M., Odenkirchen, M., Grebel, E. K., et al. 2002, AJ, 124, 349
- Sanders, J. L., & Binney, J. 2013, MNRAS, 433, 1826
- Sanders, J. L., Bovy, J., & Erkal, D. 2016, MNRAS, 457, 3817
- Spitzer, L., Jr. 1969, ApJ, 158, L139
- Spitzer, L. 1987, Princeton, NJ, Princeton University Press, 1987, 191 p.,
- Yoon, J. H., Johnston, K. V., & Hogg, D. W. 2011, ApJ, 731, 58
- Whitmore, B. C., Zhang, Q., Leitherer, C., et al. 1999, AJ, 118, 1551